A Fully Inkjet-Printed Flexible Microwave Multiresonator Circuit for Concentration Measurements of Liquid Solutions

Zonghao Li* and Sharmistha Bhadra
Department of Electrical and Computer Engineering, McGill University, Montreal, Canada
*Contact: zonghao.li@mail.mcgill.ca

***Abstract*—A fully inkjet-printed flexible microwave multiresonator circuit is presented. It is based on a coplanar waveguide (CPW) coupled to three spiral resonators to create resonances in the frequency domain. The circuit is applied for the concentration measurements of binary liquid mixtures by characterizing the insertion loss response. Water/sodium-chloride concentrations (NaCl) in the range of [0, 100] μg/ml with an increment of 10 μg/ml per sample are measured in room temperature. Two parameters are used to quantify the sensitivity, the change of the insertion loss at the resonant frequency $|\Delta S_{21}|$, and the shift of the resonant frequency $|\Delta f_{res}|$. $|\Delta S_{21}| = 0.03$ dB/(μg/ml) and $|\Delta f_{res}| = 0.25$ MHz/(μg/ml) have been achieved by the circuit within the concentration range of [0, 60] and [0, 100] μg/ml, respectively.**

I. Introduction

Microwave techniques for sensing liquid solutions have been studied numerously for applications such as food, beverage, medicine manufacturing and even oil industry due to their prompt and accurate response, fine accuracy, non-invasive and non-destructive natures [1]. In these techniques the variation of the concentration produces a change of the resonant frequency and quality factor (Q-factor), which provides an easy approach to analyze the liquid solutions [2].

Several liquid compound sensors based on the microwave resonators have been reported in various literature. The rectangular-waveguide resonator designed in [2] using TE_{101} mode has achieved a very high sensitivity for both water/NaCl and water-sucrose binary solutions. However, the structure of the rectangular waveguide is bulky and its fabrication method is not suitable for mass production. The cylindrical resonator using TE_{010} mode has been studied in [3], which relies on the return loss response to measure the concentrations for different binary liquid solutions. Planar microwave resonator structure is another popular choice for liquid sensing. In [4], a microstrip line coupled with a complementary split-ring resonator (CSRR) is employed to sense the water-ethanol solution with different concentrations. The solutions are passed through the polydimethylsiloxane (PDMS) microfluidic channel on one edge of the CSRR, and the flow will directly contact the resonator. In [5] the testing liquid sample has to be placed in a cavity on the resonator. This makes the system inappropriate for monitoring continuous liquid flow, and the inevitable residual liquid within the cavity will cause the drift error. Other planar structure sensors are reported in [6], [7], where the sensor microfabrication in the former leads to a higher cost in the prototyping process. To our knowledge, only the liquid sensor in [8] has been reported to be fully printed and flexible. Nevertheless, all above-mentioned sensors require a wired connection to a data readout unit, making them unsuitable for embedded applications. Some designs utilize active components to further improve the accuracy and sensitivity of the sensors. In [9] an active feedback loop with an amplifier is employed to enhance the Q-factor of the sensor, and a voltage-controlled oscillator with a very high Q-factor is used to analyze organic liquids by monitoring the shift of resonant frequency in [10]. Active sensors demonstrate better accuracy and sensitivity. However, the requirement of power supply leads to the necessity of battery replacement, not ideal for the long-term and embedded monitoring.

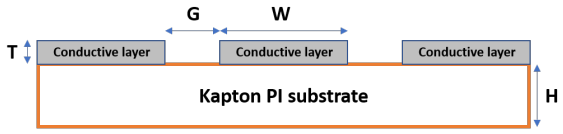

Fig. 1: CPW cross section view, where T = 50 μm, H = 5 mil, W = 5 mm, and G = 0.3 mm.

In this work, a fully inkjet-printed flexible microwave multiresonator circuit is presented for application of concentration measurements of liquid solutions. The circuit consists of a CPW coupled to three spiral resonators, which can be used for the liquid sensing. For the proof of concept, one resonator is used for the concentration measurements of water/NaCl solutions by monitoring the changes from the resonator's insertion loss response. All simulations are done in ANSYS HFSS, and all measurements are collected from the vector network analyzer (VNA, Keysight E5063A).

II. Printed Flexible Microwave Multiresonator Circuit

A. Reviews on CPW Transmission Line

To achieve a 50 Ω characteristic impedance system, a flexible printed microstrip line will have an impractical and non-achievable resolution requirement for the printer [11], which motivates us to use the CPW structure. Fig. 1 shows the cross-section view of the CPW transmission line used in our design.

The derivation of the CPW characteristic impedance in [12] using the conformal mapping assuming the substrate and the conductor thickness to be infinitely thick and thin, respectively. When the conductor thickness is comparable to the substrate (T = 50 μm and H = 127 μm), we need to revise the formulation for the CPW characteristic impedance.

Considering a conventional CPW transmission line on a dielectric substrate with a finite thickness, its characteristic impedance can be derived as [13]

$$Z_0 = \frac{30\pi}{\sqrt{\epsilon_{eff}}} \frac{K(k_1^{'})}{K(k_1)} \tag{1}$$

$$\epsilon_{eff} = 1 + \frac{(\epsilon_r - 1)}{2} \frac{K(k_2)}{K(k_2^{'})} \frac{K(k_1^{'})}{K(k_1)} \tag{2}$$

An accurate expression of the ration $K(k)/K^{'}(k)$ [14]

$$\frac{K(k)}{K^{'}(k)} = \begin{cases} \dfrac{\pi}{ln(\dfrac{2(1+\sqrt{k^{'}})}{1-\sqrt{k^{'}}})} & \text{for} \quad 0 \leq k \leq 0.707 \\ \dfrac{1}{\pi} ln \dfrac{2(1+\sqrt{k})}{1-\sqrt{k}} & \text{for} \quad 0.707 \leq k \leq 1 \end{cases} \tag{3}$$

$$k_1 = \frac{W^{'}}{W^{'} + 2G^{'}} \quad \text{and} \quad k_1^{'} = \sqrt{1 - k_1} \tag{4}$$

$$k_2 = \frac{sinh(\pi W^{'}/4H)}{sinh(\pi(W^{'} + 2G^{'})/4H)} \quad \text{and} \quad k_2^{'} = \sqrt{1 - k_2} \tag{5}$$

where ϵ_r is the dielectric constant of the substrate, ϵ_{eff} is the effective dielectric constant, and $K(k)$ represents the complete elliptic integral to the corresponding modulus k. $W^{'}$ and $G^{'}$ are the modified width and gap after taking the effect of finite metallization thickness into account [15].

$$W^{'} = W + \Delta \quad \text{and} \quad G^{'} = G - \Delta \tag{6}$$

$$\frac{\Delta}{T} = \frac{1}{\pi} \left(4.089 + \left(0.9536 + 3.864 \times 10^{-3} (\frac{b}{T}) \right) ln(\frac{4\pi G}{T}) \right) \tag{7}$$

Where $b = W/2 + G$, and Δ accounts for the metallization thickness effect. The above equations take the thickness of both substrate and metallization into consideration and yield a better result. G = 0.3 mm and W = 5 mm are the optimized dimensions for the CPW line that support the printer resolution as well as provide a characteristic impedance close to 50 Ω at 4 GHz (calculated characteristic impedance is 53 Ω). To further justify our calculation, we simulated our CPW design in HFSS and printed out the design on the flexible Kapton PI substrate. Fig. 3 shows the characteristic impedance after the S-parameter transformation from the HFSS simulation and the VNA measurement result. A characteristic impedance of about 45±2Ω has been almost achieved across the bandwidth of interest in both results, which slightly deviates to the analytic calculation. Besides the inaccurate printing process,

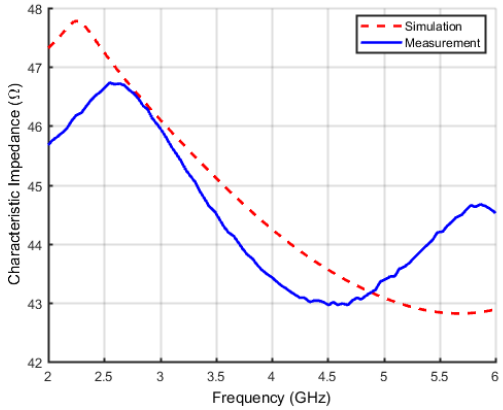

Fig. 2: Characteristic impedance of CPW with G = 0.3 mm and W = 5mm across the interested bandwidth.

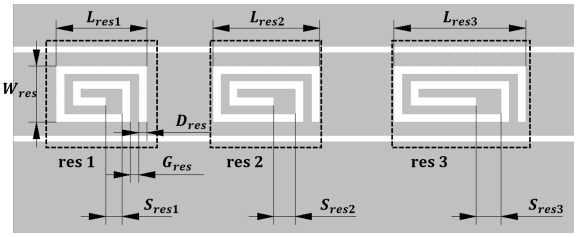

Fig. 3: Spiral resonator design, where the grey area is the conductive layer. All resonators ("res 1", "res 2" and "res 3") are centered within the CPW. L_{res1} = 5.5, L_{res2} = 6.5, L_{res3} = 8, S_{res1} = 1, S_{res2} = 1.3, S_{res3} = 1.5, W_{res} = 3.4, and D_{res} = G_{res} = 0.5, all in millimeter, and the last three parameters are the same for all resonators. From left to right, the resonators are simulated to resonate at 5.1, 4.4 and 3.5 GHz, respectively.

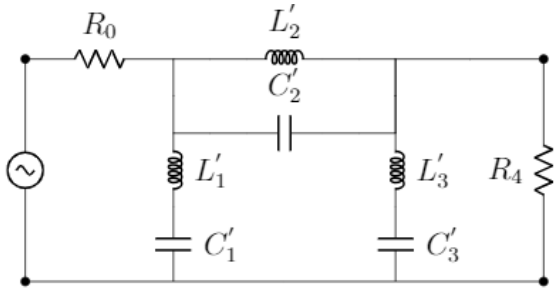

Fig. 4: Equivalent lossless circuit model of the CPW coupled to the three resonators, where R_0 = R_4 = 50 Ω, $L_1^{'}$ = 132 nH, $C_1^{'}$ = 15.3 fF, $L_2^{'}$ = 89.8 pH, $C_2^{'}$ = 14.43 pF, $L_3^{'}$ = 113.7 nH, and $C_3^{'}$ = 8.7 fF.

since the provided electrical properties of the substrate and the conductive ink are both measured in low frequency, it is reasonable to see some tolerable deviations in Fig. 2 and later simulation-versus-measurement figures. A 127 μm Dupton Kapton Polyimide film is chosen as the flexible substrate due to its excellent electrical properties ($\epsilon_r = 3.4$ and $tan\delta = 0.002$). The flexible conductive ink (σ = 1×10^6 S/m) and the inkjet printer are from Voltera. The inkjet printer has a supported resolution of 200 μm and a deposited ink thickness of around 50 μm. Fig. 1 shows the cross-section view of the CPW with $Z_0 = 50$ Ω.

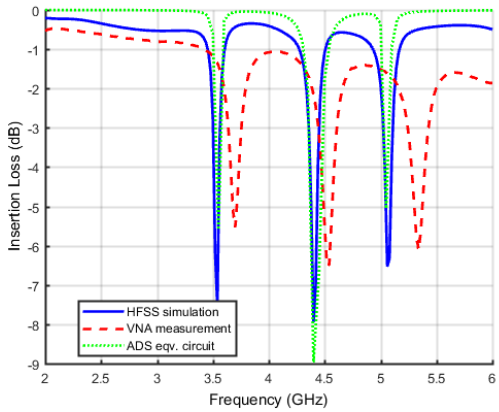

Fig. 5: Insertion loss of the CPW coupled to the three resonators, obtained from the HFSS simulation, VNA measurement, and ADS simulation of the equivalent circuit.

B. Multiresonator Design

The idea of encoding the information in the insertion loss response is to use multiple resonators coupled to the CPW. Fig. 3 shows the layout of the resonator design, where three spiral resonators locate within the CPW transmission line to create a 3-bit spectrum signature. Advanced Design Studio (ADS) is used to extract its equivalent circuit model from the HFSS simulation result based on the Chebyshev low pass filter prototype (Fig. 4) [16]. The insertion loss of the equivalent circuit model is plotted together with the HFSS simulation result and VNA measurement of the printed prototype design in Fig. 5. The resonances of the equivalent circuit can be calculated by

$$\omega_{res} = \frac{1}{\sqrt{L_n' C_n'}} \quad \text{and} \quad n = 1, 2, 3. \tag{8}$$

Depending on the topology (series and shunt) of the inductor and capacitor, the Q-factor of each resonance is [17]

$$\begin{cases} Q_{series} = R_0 \sqrt{\dfrac{C_n'}{L_n'}} & \text{for} \quad n = 1, 3. \\ Q_{shunt} = R_0 \sqrt{\dfrac{L_n'}{C_n'}} & \text{for} \quad n = 2. \end{cases} \tag{9}$$

where

$$\begin{cases} L_n' = \dfrac{R_0}{\omega_n \Delta C_n} \quad \text{and} \quad C_n' = \dfrac{\Delta C_n}{\omega_n R_0} & \text{for} \quad n = 1, 3. \\ L_n' = \dfrac{\Delta L_n R_0}{\omega_n} \quad \text{and} \quad C_n' = \dfrac{1}{\omega_n \Delta L_n R_0} & \text{for} \quad n = 2. \end{cases} \tag{10}$$

for a 50 Ω system, $R_0 = R_4 = 50\ \Omega$; ω_n is the resonant frequency created by each corresponding LC circuit; Δ is the fractional bandwidth of the stopband; and the values for L_n and C_n are the Chebyshev coefficients that can be found in [18].

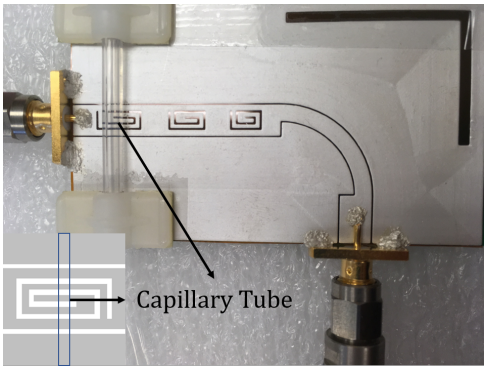

Fig. 6: Experiment set up for the concentration measurements.

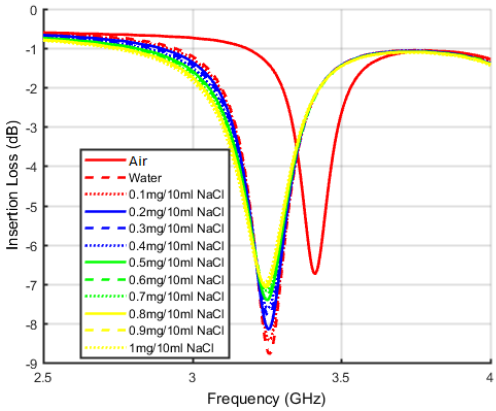

Fig. 7: Insertion loss response of the resonator "res 3" versus various water/NaCl solutions with different concentrations.

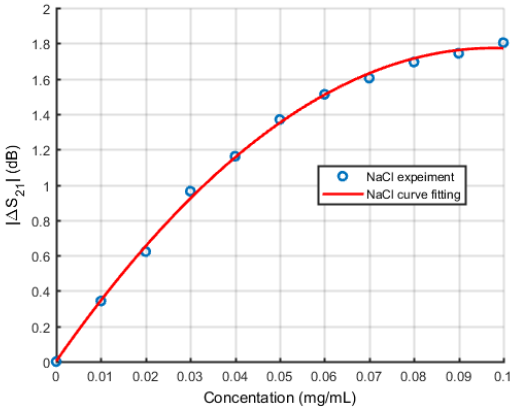

Fig. 8: Measured $|\Delta S_{21}|$ variation with NaCl concentrations in the range [0, 100] μg/ml with an increment of 10 μg/ml per sample.

It can be seen that three plots in Fig. 5 are matching to each other closely, with some tolerable deviations caused by the uneven printing process. Three notches around 3.6, 4.5 and 5.3 GHz have been observed from the measurement that is generated by "res 3", "res 2" and "res 1", respectively. Therefore, the resonant frequency increases with the dimension shrinkage of the resonator. Three resonances render a 3-bit spectrum signature.

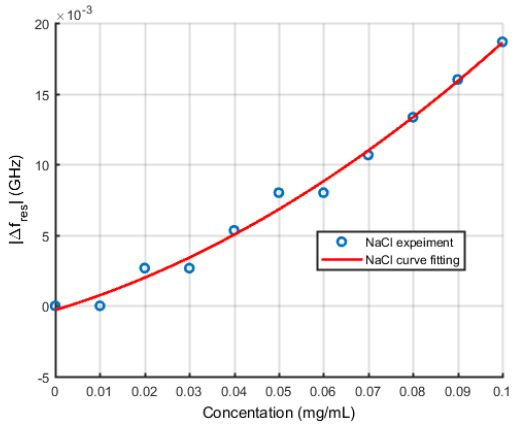

Fig. 9: Measured $|\Delta f_{res}|$ variation with NaCl concentrations in the range [0, 100] μg/ml with an increment of 10 μg/ml per sample.

III. Concentration Measurements of Liquid Solutions

Fig. 6 shows the experiment set up for the concentration measurements. The silver epoxy is used to connect the SMA connectors to the circuit. The whole circuit is with a 70 $\times$ 40 mm^2 dimension, where a capillary tube with an inner radius 0.75 mm is centered on the top of the resonator "res 3" to achieve a better sensitivity. The water/NaCl is drained and filled the tube with a syringe, where the NaCl concentration is varied in the range [0, 100] μg/ml with an increment of 10 μg/ml per sample.

Fig. 7 shows the insertion loss response of "res 3" for different NaCl concentrations, where a noticeable Q-factor degeneration is caused by the increase of the NaCl concentration. To extract the correlation between the concentration variation and the corresponding insertion loss response of water/NaCl mixtures, the amplitude change of the insertion loss at the resonant frequency $|\Delta S_{21}|$ and the resonant frequency shift $|\Delta f_{res}|$ will be analyzed. The definitions of $|\Delta S_{21}|$ and $|\Delta f_{res}|$ are defined mathematically as

$$\begin{cases} |\Delta S_{21}| = |S_{21,liquid} - S_{21,water}| \\ |\Delta f_{res}| = |f_{liquid} - f_{water}| \end{cases} \quad (11)$$

where $S_{21,liquid}$ and f_{liquid} represent the insertion loss at the resonant frequency and resonant frequency of different concentration liquid samples, respectively. $S_{21,water}$ and f_{water} are the insertion loss at the resonant frequency and resonant frequency of pure water.

The change of the insertion loss at the resonant frequency $|\Delta S_{21}|$ is plotted in Fig. 8, together with a second-order curve fitting. $|\Delta S_{21}|$ monotonically increases within the testing concentration range, showing a good linear correlation before 60 μg/ml, after which the sensitivity starts to degrade. An average 0.03 dB/(μg/ml) sensitivity is achieved before 60 μg/ml. Fig. 9 presents the shift of the resonant frequency $|\Delta f_{res}|$ that monotonically increases with the increase of NaCl concentrations. It demonstrates a better linearity than the $|\Delta S_{21}|$ plot, with a very small resonant frequency change for each concentration increment, showing a sensitivity of 0.25 MHz/(μg/ml) over the concentration range [0, 100] μg/ml. The water/NaCl solutions cause a more noticeable Q-factor change than the shift of resonant frequency, as the complex permittivity of different liquids has a different impact on them [4].

IV. Conclusion

A fully inkjet-printed flexible microwave multiresonator circuit is used for concentration measurements of water/NaCl solutions. The insertion loss response of the circuit demonstrates a high sensitivity towards a very small concentration increment. $|\Delta S_{21}|$ and $|\Delta f_{res}|$ both provide good correlations with the concentration variation.

References

[1] O. Lund Bo and E. Nyfors, "Application of microwave spectroscopy for the detection of water fraction and water salinity in water/oil/gas," *Journal of Non-Crystalline Solids*, vol. 305, pp. 345–353, 07 2002.

[2] G. Gennarelli, S. Romeo, M. R. Scarfi, and F. Soldovieri, "A microwave resonant sensor for concentration measurements of liquid solutions," *IEEE Sensors Journal*, vol. 13, no. 5, pp. 1857–1864, May 2013.

[3] B. Kapilevich and B. Litvak, "Microwave sensor for accurate measurements of water solution concentrations," in *2007 Asia-Pacific Microwave Conference*, Dec 2007, pp. 1–4.

[4] A. Ebrahimi, W. Withayachumnankul, S. Al-Sarawi, and D. Abbott, "High-sensitivity metamaterial-inspired sensor for microfluidic dielectric characterization," *IEEE Sensors Journal*, vol. 14, no. 5, pp. 1345–1351, May 2014.

[5] S. Harnsoongnoen and A. Wanthong, "Coplanar waveguides loaded with a split ring resonator-based microwave sensor for aqueous sucrose solutions," *Measurement Science and Technology*, vol. 27, no. 1, p. 015103, dec 2015. [Online]. Available: https://doi.org/10.1088%2F0957-0233%2F27%2F1%2F015103

[6] T. Chretiennot, D. Dubuc, and K. Grenier, "A microwave and microfluidic planar resonator for efficient and accurate complex permittivity characterization of aqueous solutions," *IEEE Transactions on Microwave Theory and Techniques*, vol. 61, no. 2, pp. 972–978, Feb 2013.

[7] A. A. Abduljabar, D. J. Rowe, A. Porch, and D. A. Barrow, "Novel microwave microfluidic sensor using a microstrip split-ring resonator," *IEEE Transactions on Microwave Theory and Techniques*, vol. 62, no. 3, pp. 679–688, March 2014.

[8] A. Chahadih, P. Y. Cresson, Z. Hamouda, S. Gu, C. Mismer, and T. Lasri, "Microwave/microfluidic sensor fabricated on a flexible kapton substrate for complex permittivity characterization of liquids," *Sensors and Actuators A: Physical*, vol. 229, pp. 128 – 135, 2015. [Online]. Available: http://www.sciencedirect.com/science/article/pii/S0924424715001508

[9] M. H. Zarifi, M. Rahimi, M. Daneshmand, and T. Thundat, "Microwave ring resonator-based non-contact interface sensor for oil sands applications," *Sensors and Actuators B: Chemical*, vol. 224, pp. 632 – 639, 2016. [Online]. Available: http://www.sciencedirect.com/science/article/pii/S092540051530527X

[10] V. Sekar, W. J. Torke, S. Palermo, and K. Entesari, "A self-sustained microwave system for dielectric-constant measurement of lossy organic liquids," *IEEE Transactions on Microwave Theory and Techniques*, vol. 60, no. 5, pp. 1444–1455, May 2012.

[11] H. R. Khaleel, H. M. Al-Rizzo, D. G. Rucker, and S. Mohan, "A compact polyimide-based uwb antenna for flexible electronics," *IEEE Antennas and Wireless Propagation Letters*, vol. 11, pp. 564–567, 2012.

[12] C. P. Wen, "Coplanar waveguide: A surface strip transmission line suitable for nonreciprocal gyromagnetic device applications," *IEEE Transactions on Microwave Theory and Techniques*, vol. 17, no. 12, pp. 1087–1090, December 1969.

[13] R. N. Simons, *Conventional Coplanar Waveguide*. IEEE, 2001. [Online]. Available: https://ieeexplore.ieee.org/xpl/articleDetails.jsp?arnumber=5237467

[14] W. Hilberg, "From approximations to exact relations for characteristic impedances," *IEEE Transactions on Microwave Theory and Techniques*, vol. 17, no. 5, pp. 259–265, May 1969.
[15] R. G. K. C. Gupta and I. J. Bahl, *Coplanar Lines: Coplanar Waveguide and Coplanar Strips*. Artech House, 2013.
[16] J.-S. Lim, C.-S. Kim, Y.-T. Lee, D. Ahn, and S. Nam, "A spiral-shaped defected ground structure for coplanar waveguide," *IEEE Microwave and Wireless Components Letters*, vol. 12, no. 9, pp. 330–332, Sept 2002.
[17] D. M. Pozar, *Microwave Engineering*. John Wiley & Sons, 2012, ch. 8, pp. 413–414.
[18] L. Y. G. L. Matthaei and E. M. T. Jones, *Microwave Filters, Impedance-Matching Networks, and Coupling Structures*. Artech House, 1980.